Research Article | Vol. 9, No. 4 | 1 Apr 2018 | BIOMEDICAL OPTICS EXPRESS 1590
Biomedical Optics EXPRESS

Identifying intestinal fibrosis and inflammation by spectroscopic photoacoustic imaging: an animal study *in vivo*

YUNHAO ZHU,[1,2] LAURA A. JOHNSON,[3] ZIYI HUANG,[4] JONATHAN M. RUBIN,[5] JIE YUAN,[1] HAO LEI,[6] JUN NI,[6] XUEDING WANG,[2] PETER D. R. HIGGINS,[3] AND GUAN XU[5,*]

[1]*Department of Electronic Science and Engineering, Nanjing University, Nanjing, Jiangsu 21000, China*
[2]*Department of Biomedical Engineering, University of Michigan, Ann Arbor, MI 48109, USA*
[3]*Department of Internal Medicine, University of Michigan Medical School, Ann Arbor, MI 48109, USA*
[4]*Department of Electrical and Computer Engineering, University of Michigan, Ann Arbor, MI 48109, USA*
[5]*Department of Radiology, University of Michigan Medical School, Ann Arbor, MI 48109, USA*
[6]*Department of Mechanical Engineering, University of Michigan, Ann Arbor, MI 48109, USA*
**guanx@med.umich.edu*

Abstract: Crohn's disease (CD) is a chronic autoimmune disease characterized by obstructing intestinal strictures. Conventional imaging modalities can identify the strictures but cannot characterize whether a stricture is predominantly inflammatory or fibrotic. The purpose of this study is to examine the capability of photoacoustic (PA) imaging to characterize intestinal fibrosis and inflammation *in vivo*. Intestinal strictures in a rat model of CD were imaged with a PA-ultrasound parallel imaging system. Internal and external illuminations were attempted, both with transcutaneous PA signal reception. The PA signal magnitudes acquired at wavelengths targeting individual molecular components and the derived functional information showed significant differences between the inflammatory and fibrotic strictures, consistent with histological inflammation and fibrosis.

OCIS codes: (170.3880) Medical and biological imaging; (170.5120) Photoacoustic imaging; (170.7170) Ultrasound; (170.6510) Spectroscopy, tissue diagnostics.

References and links

1. G. R. Lichtenstein, A. Olson, S. Travers, R. H. Diamond, D. M. Chen, M. L. Pritchard, B. G. Feagan, R. D. Cohen, B. A. Salzberg, S. B. Hanauer, and W. J. Sandborn, "Factors Associated with the Development of Intestinal Strictures or Obstructions in Patients with Crohn's Disease," Am. J. Gastroenterol. **101**(5), 1030–1038 (2006).
2. G. Oberhuber, P. C. Stangl, H. Vogelsang, E. Schober, F. Herbst, and C. Gasche, "Significant association of strictures and internal fistula formation in Crohn's disease," Virchows Arch. **437**(3), 293–297 (2000).
3. I. C. Lawrance, C. J. Welman, P. Shipman, and K. Murray, "Correlation of MRI-determined small bowel Crohn's disease categories with medical response and surgical pathology," World J. Gastroenterol. **15**(27), 3367–3375 (2009).
4. E. V. Loftus, Jr., P. Schoenfeld, and W. J. Sandborn, "The epidemiology and natural history of Crohn's disease in population-based patient cohorts from North America: a systematic review," Aliment. Pharmacol. Ther. **16**(1), 51–60 (2002).
5. R. D. Cohen, L. R. Larson, J. M. Roth, R. V. Becker, and L. L. Mummert, "The cost of hospitalization in Crohn's disease," Am. J. Gastroenterol. **95**(2), 524–530 (2000).
6. S. Kugathasan, L. A. Denson, T. D. Walters, M.-O. Kim, U. M. Marigorta, M. Schirmer, K. Mondal, C. Liu, A. Griffiths, J. D. Noe, W. V. Crandall, S. Snapper, S. Rabizadeh, J. R. Rosh, J. M. Shapiro, S. Guthery, D. R. Mack, R. Kellermayer, M. D. Kappelman, S. Steiner, D. E. Moulton, D. Keljo, S. Cohen, M. Oliva-Hemker, M. B. Heyman, A. R. Otley, S. S. Baker, J. S. Evans, B. S. Kirschner, A. S. Patel, D. Ziring, B. C. Trapnell, F. A. Sylvester, M. C. Stephens, R. N. Baldassano, J. F. Markowitz, J. Cho, R. J. Xavier, C. Huttenhower, B. J. Aronow, G. Gibson, J. S. Hyams, and M. C. Dubinsky, "Prediction of complicated disease course for children newly diagnosed with Crohn's disease: a multicentre inception cohort study," Lancet **389**(10080), 1710–1718 (2017).

#318889 https://doi.org/10.1364/BOE.9.001590
Journal © 2018 Received 8 Jan 2018; revised 23 Feb 2018; accepted 26 Feb 2018; published 8 Mar 2018

Biomedical Optics EXPRESS

7. E. Domènech, M. Mañosa, and E. Cabré, "Top-Down Therapy: Is the Evidence Strong Enough?" Dig. Dis. **27**(3), 306–311 (2009).
8. F. Rieder, I. C. Lawrance, A. Leite, and M. Sans, "Predictors of fibrostenotic Crohn's disease," Inflamm. Bowel Dis. **17**(9), 2000–2007 (2011).
9. S. M. Dandalides, W. D. Carey, R. Petras, and E. Achkar, "Endoscopic small bowel mucosal biopsy: a controlled trial evaluating forceps size and biopsy location in the diagnosis of normal and abnormal mucosal architecture," Gastrointest. Endosc. **35**(3), 197–200 (1989).
10. K. Kim, L. A. Johnson, C. Jia, J. C. Joyce, S. Rangwalla, P. D. R. Higgins, and J. M. Rubin, "Noninvasive Ultrasound Elasticity Imaging (UEI) of Crohn's Disease: Animal Model," Ultrasound Med. Biol. **34**(6), 902–912 (2008).
11. D. A. Fisher, J. T. Maple, T. Ben-Menachem, B. D. Cash, G. A. Decker, D. S. Early, J. A. Evans, R. D. Fanelli, N. Fukami, J. H. Hwang, R. Jain, T. L. Jue, K. M. Khan, P. M. Malpas, R. N. Sharaf, A. K. Shergill, and J. A. Dominitz; ASGE Standards of Practice Committee, "Complications of colonoscopy," Gastrointest. Endosc. **74**(4), 745–752 (2011).
12. Z. Tarján, G. Tóth, T. Györke, A. Mester, K. Karlinger, and E. K. Makó, "Ultrasound in Crohn's disease of the small bowel," Eur. J. Radiol. **35**(3), 176–182 (2000).
13. P. Paolantonio, R. Ferrari, F. Vecchietti, S. Cucchiara, and A. Laghi, "Current status of MR imaging in the evaluation of IBD in a pediatric population of patients," Eur. J. Radiol. **69**(3), 418–424 (2009).
14. M. Boudiaf, P. Soyer, C. Terem, J. P. Pelage, E. Maissiat, and R. Rymer, "Ct Evaluation of Small Bowel Obstruction," Radiographics **21**(3), 613–624 (2001).
15. J. M. Esteban, L. Maldonado, V. Sanchiz, M. Minguez, and A. Benages, "Activity of Crohn's disease assessed by colour Doppler ultrasound analysis of the affected loops," Eur. Radiol. **11**(8), 1423–1428 (2001).
16. J. Rimola, N. Planell, S. Rodríguez, S. Delgado, I. Ordás, A. Ramírez-Morros, C. Ayuso, M. Aceituno, E. Ricart, A. Jauregui-Amezaga, J. Panés, and M. Cuatrecasas, "Characterization of Inflammation and Fibrosis in Crohn's Disease Lesions by Magnetic Resonance Imaging," Am. J. Gastroenterol. **110**(3), 432–440 (2015).
17. R. W. Stidham and P. D. R. Higgins, "Imaging of intestinal fibrosis: current challenges and future methods," United European Gastroenterol. J. **4**(4), 515–522 (2016).
18. L. V. Wang and S. Hu, "Photoacoustic Tomography: *In Vivo* Imaging from Organelles to Organs," Science **335**(6075), 1458–1462 (2012).
19. X. Wang, Y. Pang, G. Ku, X. Xie, G. Stoica, and L. V. Wang, "Noninvasive laser-induced photoacoustic tomography for structural and functional *in vivo* imaging of the brain," Nat. Biotechnol. **21**(7), 803–806 (2003).
20. H. Lei, L. A. Johnson, S. Liu, D. S. Moons, T. Ma, Q. Zhou, M. D. Rice, J. Ni, X. Wang, P. D. Higgins, and G. Xu, "Characterizing intestinal inflammation and fibrosis in Crohn's disease by photoacoustic imaging: feasibility study," Biomed. Opt. Express **7**(7), 2837–2848 (2016).
21. F. Knieling, C. Neufert, A. Hartmann, J. Claussen, A. Urich, C. Egger, M. Vetter, S. Fischer, L. Pfeifer, A. Hagel, C. Kielisch, R. S. Görtz, D. Wildner, M. Engel, J. Röther, W. Uter, J. Siebler, R. Atreya, W. Rascher, D. Strobel, M. F. Neurath, and M. J. Waldner, "Multispectral Optoacoustic Tomography for Assessment of Crohn's Disease Activity," N. Engl. J. Med. **376**(13), 1292–1294 (2017).
22. J. Yuan, G. Xu, Y. Yu, Y. Zhou, P. L. Carson, X. Wang, and X. Liu, "Real-time photoacoustic and ultrasound dual-modality imaging system facilitated with graphics processing unit and code parallel optimization," J. Biomed. Opt. **18**(8), 086001 (2013).
23. G. Xu, Z. X. Meng, J. D. Lin, C. X. Deng, P. L. Carson, J. B. Fowlkes, C. Tao, X. Liu, and X. Wang, "High resolution physio-chemical tissue analysis: towards non-invasive *in vivo* biopsy," Sci. Rep. **6**(1), 16937 (2016).
24. J. R. Dillman, R. W. Stidham, P. D. R. Higgins, D. S. Moons, L. A. Johnson, and J. M. Rubin, "US Elastography-derived Shear Wave Velocity Helps Distinguish Acutely Inflamed from Fibrotic Bowel in a Crohn Disease Animal Model," Radiology **267**(3), 757–766 (2013).
25. R. W. Stidham, J. Xu, L. A. Johnson, K. Kim, D. S. Moons, B. J. McKenna, J. M. Rubin, and P. D. R. Higgins, "Ultrasound Elasticity Imaging for Detecting Intestinal Fibrosis and Inflammation in Rats and Humans with Crohn's Disease," Gastroenterology **141**(3), 819–826.e1 (2011).
26. G. Xu, Z. X. Meng, J. D. Lin, C. X. Deng, P. L. Carson, J. B. Fowlkes, C. Tao, X. Liu, and X. Wang, "High resolution Physio-chemical Tissue Analysis: Towards Non-invasive *In Vivo* Biopsy," Sci. Rep. **6**(1), 16937 (2016).
27. H.-W. Wang, N. Chai, P. Wang, S. Hu, W. Dou, D. Umulis, L. V. Wang, M. Sturek, R. Lucht, and J.-X. Cheng, "Label-Free Bond-Selective Imaging by Listening to Vibrationally Excited Molecules," Phys. Rev. Lett. **106**(23), 238106 (2011).
28. H. Zhang, W. Y. Chao, Q. Cheng, S. Huang, X. Wang, D. Wu, and G. Xu, "Interstitial photoacoustic spectral analysis: instrumentation and validation," Biomed. Opt. Express **8**(3), 1689–1697 (2017).
29. R. George and L. J. Walsh, "Performance assessment of novel side firing flexible optical fibers for dental applications," Lasers Surg. Med. **41**(3), 214–221 (2009).
30. H. K. Hughes, "Beer's Law and the Optimum Transmittance in Absorption Measurements," Appl. Opt. **2**(9), 937–945 (1963).
31. W. F. Cheong, S. A. Prahl, and A. J. Welch, "A review of the optical properties of biological tissues," Quantum Electronics, IEEE Journal of **26**(12), 2166–2185 (1990).
32. S. L. Jacques, "Optical properties of biological tissues: a review," Phys. Med. Biol. **58**(11), R37–R61 (2013).

Biomedical Optics EXPRESS

33. C. P. Sabino, A. M. Deana, T. M. Yoshimura, D. F. T. da Silva, C. M. França, M. R. Hamblin, and M. S. Ribeiro, "The optical properties of mouse skin in the visible and near infrared spectral regions," J. Photochem. Photobiol. B **160**, 72–78 (2016).
34. X. Wang, X. Xie, G. Ku, L. V. Wang, and G. Stoica, "Noninvasive imaging of hemoglobin concentration and oxygenation in the rat brain using high-resolution photoacoustic tomography," J. Biomed. Opt. **11**(2), 024015 (2006).
35. Z. Yuan, Q. Wang, and H. Jiang, "Reconstruction of optical absorption coefficient maps of heterogeneous media by photoacoustic tomography coupled with diffusion equation based regularized Newton method," Opt. Express **15**(26), 18076–18081 (2007).
36. D. F. Higgins, K. Kimura, M. Iwano, and V. H. Haase, "Hypoxia-inducible factor signaling in the development of tissue fibrosis," Cell Cycle **7**(9), 1128–1132 (2008).
37. S. Leungwattanakij, T. J. Bivalacqua, M. F. Usta, D.-Y. Yang, J.-S. Hyun, H. C. Champion, A. B. Abdel-Mageed, and W. J. G. Hellstrom, "Cavernous Neurotomy Causes Hypoxia and Fibrosis in Rat Corpus Cavernosum," J. Androl. **24**(2), 239–245 (2003).
38. J. R. Rajian, R. Li, P. Wang, and J.-X. Cheng, "Vibrational Photoacoustic Tomography: Chemical Imaging beyond the Ballistic Regime," J. Phys. Chem. Lett. **4**(19), 3211–3215 (2013).

1. Introduction

Crohn's disease (CD) is a chronic autoimmune disease characterized by obstructing intestinal strictures due to inflammation, fibrosis, or a combination of both [1, 2]. Among the estimated 700,000 CD patients in the United States [3–5], 70% suffer from irreversible fibrotic intestinal strictures and require at least one surgical intervention [5]. In addition, since extracellular matrix gene expression (ECM) is a recognized predictor of future complicated disease in CD patients, the measurement of fibrosis in CD also determines whether a patient has progression of disease [6]. As collagen is the major ECM molecule, longitudinal measurement of collagen enables measurement of disease progression and clinical response to current and novel therapeutics. Accurate measurement of intestinal fibrosis versus inflammation is critical as inflammatory strictures can be treated medically, but late stage fibrotic strictures are irreversible and have to be removed surgically. Therefore, a non-invasive method to characterize CD strictures will contribute to the therapeutic monitoring and planning for treatment of CD patients [7, 8].

The standard diagnostic procedure for CD, endoscopic biopsy [9], removes small pieces of mucosa from the inner lining of the intestine for histopathology. The inflammatory intestinal strictures are characterized by increased vascularity and inflammatory cells, whereas the fibrotic ones are characterized by extracellular collagen deposition [10]. Due to the limited sampling depth, biopsies rarely reach the muscular layers where fibrosis largely occurs. In addition, endoscopy requires sedation, temporary inability to work or drive, requires a second person to care for the patient after sedation, and has some uncommon risks including abdominal pain, perforation, hemorrhage, and infections [11]. Conventional non-invasive imaging modalities such as ultrasound (US) [12], magnetic resonance [3, 13], and X-ray imaging [1, 2, 14] have demonstrated their ability to identify strictures. However, due to their inability to assess the molecular components such as hemoglobin and collagen, these structural imaging modalities cannot currently differentiate inflammation and fibrosis in the strictures. Doppler ultrasound has shown the capability of identifying inflammation by detecting the increased blood flow due to neovasculature [15]. Unfortunately, the amount of visualized blood flow is largely independent from the amount of fibrosis and is more representative of the associated inflammation. Functional magnetic resonance imaging has been attempted for the diagnosis of bowel fibrosis [16]. However, this study was limited to differentiating severe, end-stage fibrosis. There has been no prominent evidence to support the clinical significance of these approaches [17].

Spectroscopic photoacoustic (PA) imaging combines the advantages of optical and US imaging [18, 19]. With its high sensitivity to molecular components and decent resolution as well as penetration, is an ideal candidate for characterizing intestinal strictures. We have previously demonstrated the capability of PA imaging in identifying inflammation and fibrosis in human and animal tissues *ex vivo* by quantifying the hemoglobin and collagen

Biomedical Optics EXPRESS

content, respectively [20]. A recent human subject study has shown the capability of PA imaging in assessing only intestinal inflammation [21].

The purpose of this study is to distinguish fibrotic intestinal strictures from the inflammatory *in vivo* using our PA-US parallel imaging system [22]. Illuminations targeting the strong absorption of hemoglobin and collagen have been used for characterizing inflammation and fibrosis [20, 23], respectively. An internal light source was initially implemented and external illumination was introduced later for fully transcutaneous imaging. PA signal intensities as well as functional information such as blood oxygenation and the ratio between the hemoglobin and collagen contents were quantified. PA signal intensities were compared to histological inflammation and fibrosis. Statistically significant differences were observed between the inflammatory and fibrotic intestinal strictures. In the absence of tools to non-invasively measure and discriminate inflammatory from fibrotic disease, the proposed PA imaging approach may inform clinical decision-making for managing CD.

2. Methods and materials

The animal protocol for the experiments was approved by the Institutional Animal Care and Use Committee of the University of Michigan.

2.1 Animal preparation

This study examines the proposed imaging approach as applied to the trinitrobenzene sulfonic acid (TNBS) model of Crohn's disease in rats [10, 20]. Rats weighing 175-200 grams (10-12 weeks old, Harlan Laboratories, Indianapolis, IN) were treated by procedures described in the previous studies [10, 24, 25]. In brief, acute animals were treated with a single intra-rectal dose of TNBS to induce inflammatory strictures. Chronic animals were treated with multiple cycles of escalating intra-rectal TNBS doses followed by mucosal healing which ultimately produces intestinal fibrosis. Normal (non-TNBS treated) animals were not included in this study as the normal bowel is difficult to visualize by any conventional imaging modalities, as mentioned in the introduction. The fur on the rat abdomens was shaved for improved acoustic coupling. The rats were kept under anesthesia using isoflurane inhalation during the procedures. After the imaging, the animals were euthanized by inhaling an overdose of carbon dioxide. Post-imaging, the affected bowel was harvested for histologic analysis.

2.2 Histology

Sections of distal colon tissue were collected for histology, fixed in buffered formalin for 24 h, and embedded in paraffin. Five micron sections were made for mounting on slides. Hematoxylin and eosin (H&E) staining and Masson's trichrome staining were performed by the University of Michigan Cancer Center Histology and Immunoperoxidase Lab (Ann Arbor, MI, USA) and McClinchey Histology Lab (Stockbridge, MI, USA), respectively. Digital photomicrographs of proximal and distal colon sections were captured using an Olympus BX51 microscope at the University of Michigan Microscopy and Image Analysis Laboratory (Ann Arbor, MI, USA).

2.3 Experiment systems

Our previously developed PA-US parallel imaging system [22] based on a research US platform (Vantage, Redmond, WA) was used to acquire all the images in this study. The illumination source of PA imaging is a tunable optical parametric oscillator (OPO) laser (VibrantB, Opotek Inc., Carlsbad, CA, USA) pumped by the second harmonic output of an Nd:YAG pulsed laser (Brilliant B, Quantel, Bozeman, MT, USA). As examined in previous studies [26, 27], PA imaging within the ranges of 532-850 nm and 1310-1370 nm provides quantitative measurements of the contents of hemoglobin and collagen, respectively. Aimed at estimating blood oxygenation, illumination at 750 and 850 nm were used, as the two wavelengths lie on either side of the intersection of oxygenated and deoxygenated

Biomedical Optics EXPRESS

hemoglobin absorption spectra at 800 nm, as shown in Fig. 1. For collagen content, 1310 nm was used as the laser provides maximum output at 1310 nm in the aforementioned range.

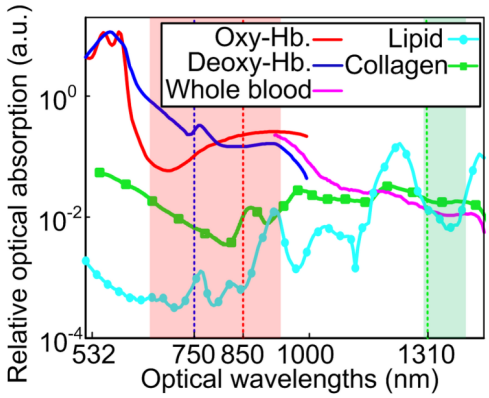

Fig. 1. Optical absorption spectra of relevant molecular components in this study. The shaded areas are the wavelengths ranges that are targeting the hemoglobin and collagen contents, respectively. Hb: Hemoglobin.

High frequency probes, CL15-7 (Philips, Andover, MA) and L22-14v (Verasonics, Seattle, WA) were selected for resolving the bowel architectures in the rats at relatively shallow depth. Both probes have 128 transducer elements. The CL15-7 has a frequency range of 7 to 15 MHz, an aperture of 23 mm and a center frequency of 9 MHz. The L22-14v has a frequency range of 14 to 22 MHz, an aperture of 12.8 mm and a center frequency of 18 MHz. The sampling rates for both probes were set as four times the center frequencies.

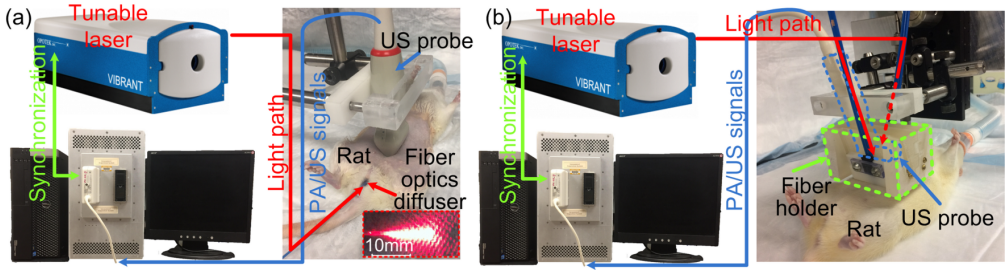

Fig. 2. The experiment setups. (a) The internal illumination delivery was achieved using a fiber optic diffuser. (b) The external illumination was delivered by integrating fiber optics to the US probe with a fiber holder. The details of the fiber holder are shown in Fig. 3.

As illustrated in Fig. 2, this study involves PA imaging with two sets of experiments with internal and external illumination, respectively. Both the US and PA images were reconstructed using delay-and-sum method and displayed in parallel in real time. The speed of sound was defined as 1540 m/s. The reconstruction pixel size was arbitrarily defined as 1/3 of the wavelength corresponding to the central frequency of each probe.

2.4 PA-US parallel imaging with endoscopic illumination

We began the study with endoscopic illumination at 1310 nm to quantify the collagen content with PA measurements. Hemoglobin content was not evaluated at this stage as PA imaging at 750 and 850 nm in small animals has been extensively investigated [18, 19]. A total of 6 acute and 6 chronic animals were examined.

The illumination was delivered through the fiber optic diffuser shown in the bottom right panel in Fig. 2(a) [28]. The fiber optic diffuser was custom-made following the procedures described in [29]. It has a diameter of 600 μm and produces relatively uniform optical density at the illumination surface, with limited weak spots due to imperfect fabrication. The fiber

Biomedical Optics EXPRESS

optics diffuser facilitates the comprehensive observation of a segment of the colon. A collimated laser beam of 8 mJ power was projected onto the coupling end of the fiber optic diffuser. The optical energy was monitored by an optical power meter for signal magnitude normalization. Considering the coupling efficiency of 50%, approximately 95 mJ/cm^2 was delivered at the illumination surface of the fiber optic diffuser, which is below the safety limit of 100 mJ/cm^2 defined by the American National Standard Institute (ANSI). The L22-14v probe was used for imaging the fiber optic diffuser along its longitudinal dimension. The fiber optic diffuser was inserted into the rat colon under the guidance of US alone. The PA imaging modality was activated and the PA and US images were acquired in parallel. 50 frames were acquired for each animal.

For the purpose of excluding the imperfect spots at the fiber optic diffuser surface and obtaining a reliable measure, the 100th to 1000th brightest pixels within the illuminated regions were spatially averaged to provide a single PA value for each frame. These frames were acquired at 10 frames per second. The PA values derived from 50 consecutive frames were then averaged over time, to minimize the uncertainty introduced by the laser energy fluctuations. The averaged PA values for each animal across 50 frames were examined by two tailed t-tests with the null hypothesis that the acute and chronic animals cannot be differentiated by the PA signal intensities.

2.5 PA-US parallel imaging with external illumination

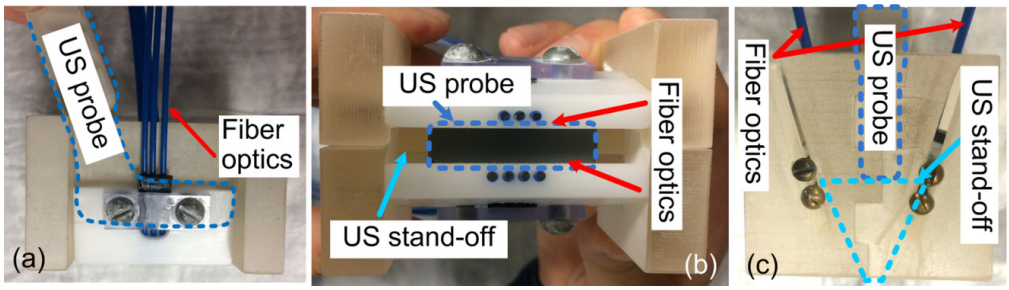

Fig. 3. PA-US parallel imaging probe (a) Side view; (b) Bottom view; (c) Front view.

The transcutaneous PA-US imaging of the intestinal strictures was performed with 5 acute and 5 chronic animals at the wavelengths of 750, 850 and 1310 nm, as shown in Fig. 2(b). Figure 3 shows the PA-US parallel imaging probe dedicated to this study. The probe contains a customized fiber optic bundle consisting of 7 optical fibers with diameters of 1mm (Thorlabs, New Jersey, US). The fiber optics were arranged to project illumination within 1 × 1 cm^2 to cover approximately central 1/2 of the imaging aperture. US coupling gel contains water which strongly attenuates optical energy at 1310 nm. Therefore, the emission ends of the fiber optics were positioned close to the skin surface. The cavity between the US probe and the skin was filled with US coupling gel and sealed with a piece of plastic membrane, forming an acoustic stand-off. The optical energy density was continuously monitored by an optical power meter at the coupling end of the fiber optic bundle and maintained below 10 mJ/cm^2 at the emission end for all wavelengths, which is below the ANSI safety limit (20mJ/cm^2 for 750 and 850 nm, 100 mJ/cm^2 for 1310 nm).

During the imaging procedures, the transverse cross-sections of the intestinal strictures were located by an US radiologist using only the US modality and positioned in the central 1/2 of the imaging aperture. The PA modality was then turned on for dual-modality imaging. The attenuation of the stool inside the intestines and the surrounding tissues introduced uncertainty to the PA signals within the far and side walls of the strictures. Therefore, the top quadrant of the bowel loops were selected as the regions of interest (ROI) and all subsequent quantifications were made to the ROI. The PA pixel intensities within the ROI in each frame

Biomedical Optics EXPRESS

were compensated by the optical attenuation of the skin and muscle layers using Eq. (1) following Beer's law [30].

$$P_{comp}(d_{skin}, d_{muscle}) = P_{meas} \div \exp\{-[\mu_{a\_skin}(\lambda) + \mu'_{s\_skin}(\lambda)] \times d_{skin} - [\mu_{a\_muscle}(\lambda) + \mu'_{s\_muscle}(\lambda)] \times d_{muscle}\} \quad (1)$$

where $\mu_a(\lambda)$ and $\mu_s'(\lambda)$ are the absorption and the reduced scattering coefficients at wavelength λ, respectively. These optical properties were reported in previous studies [31–33] and listed in Table 1. P_{comp} and P_{meas} are the measured and compensated PA signal intensities, respectively. d are the thickness of skin and muscle layers measured in the US images. The compensated PA intensities (P) within the ROI were inserted into Eq. (2), where the relative contents of oxy- and deoxy- hemoglobin and collagen were solved [34, 35]. The blood oxygenation (SpO_2) [34] and the ratio between concentrations of collagen and hemoglobin ($Collagen/Hb$) were derived using Eq. (3).

$$\begin{bmatrix} c_{HbO} \\ c_{Hb} \\ c_{Collagen} \end{bmatrix} = \begin{bmatrix} \mu_{HbO@750nm} & \mu_{Hb@750nm} & \mu_{collagen@750nm} \\ \mu_{HbO@850nm} & \mu_{Hb@850nm} & \mu_{collagen@850nm} \\ \mu_{HbO@1310nm} & \mu_{Hb@1310nm} & \mu_{collagen@1310nm} \end{bmatrix}^{-1} \times \begin{bmatrix} P_{750nm} \\ P_{850nm} \\ P_{1310nm} \end{bmatrix} \quad (2)$$

$$SpO_2 = \frac{c_{HbO}}{c_{HbO} + c_{Hb}}, \quad Collagen/Hb = \frac{c_{collagen}}{c_{HbO} + c_{Hb}} \quad (3)$$

Table 1. optical properties used for spectral unmixing and optical attenuation along the penetration depth [31–33]. Hb: Hemoglobin.

	λ = 750 nm		λ = 850 nm		λ = 1310 nm	
	μ_a (mm^{-1})	μ_s' (mm^{-1})	μ_a (mm^{-1})	μ_s' (mm^{-1})	μ_a (mm^{-1})	μ_s' (mm^{-1})
Oxy-Hb	0.11		0.23		0.011	
Deoxy-Hb	0.30		0.15		0.011	
Collagen	0.007		0.009		0.019	
Skin	0.08	0.52	0.08	0.44	0.11	0.15
Muscle	0.52	0.89	0.56	0.80	0.61	0.53

The scattering of collagen and hemoglobin are not listed here because the PA signals are only associated with the absorption of these molecular components.

For the statistical analysis, the pixel-wise quantifications were averaged within the ROI in each frame. The PA values in the neighboring 10 frames (1 second with 10Hz laser repetition rate) were averaged. Such post-processing approach was purposed at minimizing the uncertainty introduced by the animal motion. Results from the acute and chronic animals were compared in a two tailed t-test with the same null hypothesis in section 2.3.

3. Results

3.1 Histology

Figure 4 illustrates the gross pathology and histology from acute (inflammatory) and chronic (fibrotic) rat colon. In the acute model, the distal colon was grossly edematous, with characteristic submucosal hemorrhages and patchy areas of necrosis. Histopathology revealed areas of tissue ulceration, while H&E staining identified large areas of extravasated red blood cells in the lamina propria and epithelium as well as infiltration of inflammatory cells. While trichrome staining for collagen revealed edematous distortion of the normal collagen

Biomedical Optics EXPRESS

architecture, increased tissue collagen was not observed, consistent with an acute inflammatory phenotype.

In contrast, hemorrhage and tissue edema were absent in the chronic model. However, the colon exhibited marked tissue thickening and palpable stiffness as evidenced by a curled or wavy gross appearance. H&E histological analysis revealed some inflammatory cells, but no areas of extravasated red blood cells. Trichrome staining identified extensive collagen deposition, with architectural distortion of the lamina propria and muscularis layers, consistent with advanced fibrotic disease.

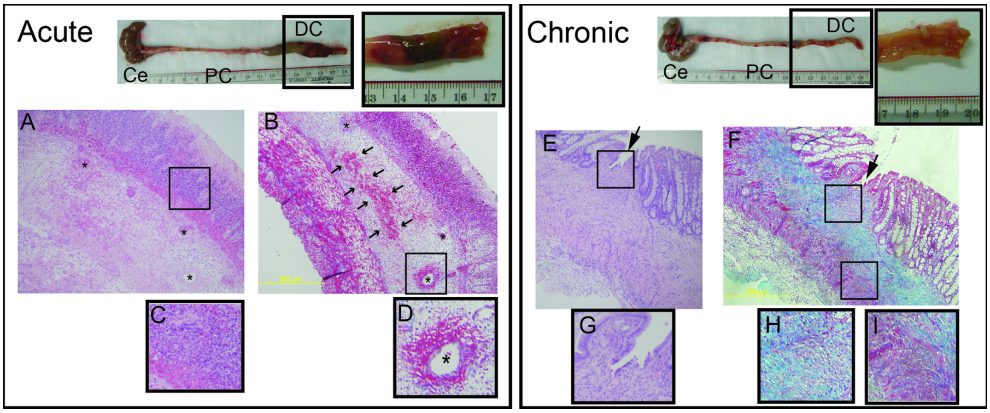

Fig. 4. Gross pathology of the cecum and colon from acute vs. chronic TNBS rats. Ce = cecum, PC = proximal colon (unaffected), DC = affected distal colon. Upper panel inset illustrates the gross luminal differences between the acute and chronic models with hemorrhagic and necrotic regions in the acute model and the thickened, contracted features characteristic of the chronic fibrosis. Histological features of the acute model (A-D). H&E staining (A) identifies increased inflammatory cells (dark blue nuclei, detailed in inset C), and large regions of extravascular red blood cells (B, arrowheads) in the acute model with red blood cell extravasation from blood vessels (asterisks, detailed in inset D). Trichrome staining (B,D) reveled structural collagen only. Large collagen deposition was not observed. In contrast, histological features of the chronic fibrosis model (E-I) demonstrated massive transmural collagen deposition without red blood cell extravasation. H & E staining revealed a healed ulcer (E, arrow) with few inflammatory cells present (inset, G). Trichrome staining (F) illustrates massive disorganized collagen deposition (blue staining, detailed in H) and architectural disruption by collagen extending into the deeper muscle layers (inset I).

3.2 PA-US parallel imaging with endoscopic illumination

Figure 5(a) shows the example images of PA-US parallel images acquired in an acute and a chronic TNBS animals. As illustrated, the longitudinal cross-section of the fiber optic diffuser is shown within the US image. Since the fiber optic diffuser was located at the inner surface of the affected intestine, the only PA signals were from the intestine. As expected, the imperfect illumination surface generated inhomogeneous PA signal intensity along the fiber optics. Figure 5(b) shows the statistics with the averaged PA signal intensities from the 6 acute and 6 chronic animals. Approximately a factor of 2 fold increase in collagen was found in chronic animals compared to the acute ones. The increased 1310 nm signal is consistent with increased collagen deposition as identified by histology (Fig. 4).

Biomedical Optics EXPRESS

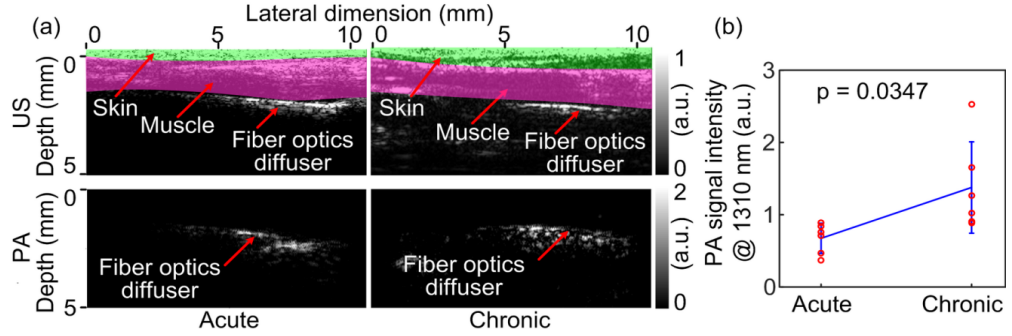

Fig. 5. PA-US parallel imaging with internal illumination. (a) shows the example images of the PA-US parallel images acquired in a chronic TNBS animal. The skin and muscle layers in the US images are shaded in green and purple. (b) shows the statistics with the quantitative values from each animal.

3.3 External illumination

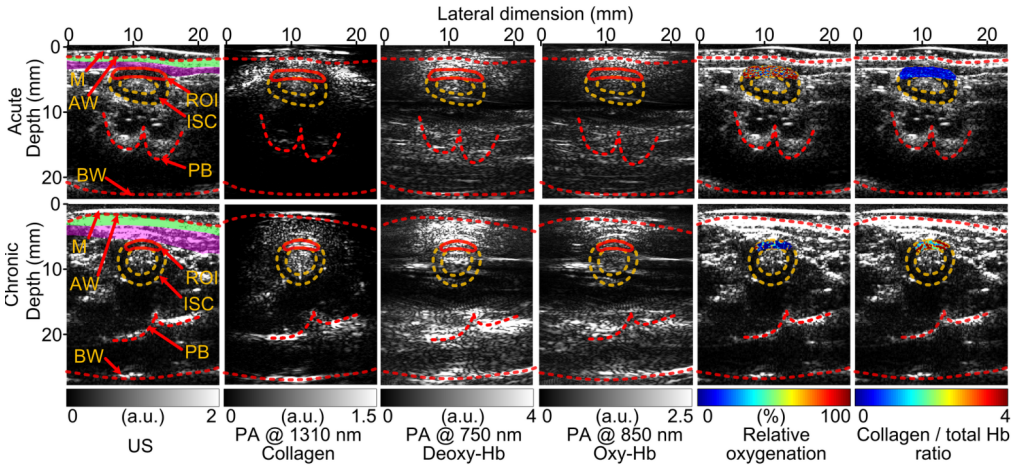

Fig. 6. The representative US and PA images within the ROIs. The top and bottom rows are acquired in acute and chronic animals, respectively. Column 1 present the US images. The green and purple shaded areas in the first column are skin and muscle layers, respectively. Columns 2-4 are PA images acquired in parallel with the US imaging at 1310, 750 and 850 respectively. Columns 5-6 are the US images with coregistered relative oxygenation and collagen/Hb ratio within the ROIs. M: Membrane supporting the acoustic stand-off. AW: Abdominal wall. BW: Back wall. ROI: Region-of-interest. ISC: Intestinal stricture cross-section. PB: Pelvic bone. Hb: Hemoglobin.

Figure 6 shows the representative US and PA images at the three wavelengths, and the derived blood oxygenation and the relative collagen and hemoglobin ratio within the ROIs coregistered on US images. Both the US and PA images of the acute animal shows less detail in deep tissue compared to the chronic one. This is because we focused on the identifying the top quadrant of the bowel loop and the probe orientation is not optimized for the deeper structures such as pelvic bone and the back body wall. The skin and muscle layers were identified in the US images in order to compensate for optical energy attenuation along depth. The abnormal bowel loop was positioned in the central 1/2 of the image aperture in order to concentrate the light over the loop. Higher PA signal intensity at 1310 nm and collagen/hemoglobin ratios were found in the chronic animals due to the deposition of extracellular collagen and decreased vascularity in the fibrotic intestinal stricture. Increased collagen deposition in the chronic animals was confirmed by trichrome staining for collagen. In contrast, higher oxygenated (850 nm) and deoxygenated (750 nm) hemoglobin and blood

Biomedical Optics EXPRESS

oxygenation levels were found in the acute animals due to the rich vascularity and blood supply secondary to the inflamed segment of intestine. In the acute animals, H&E histology identified hemorrhages and red blood cell extravasation consistent with the increased hemoglobin signal.

Figure 7 shows the statistics of the factors derived from the 5 acute and 5 chronic animals. The quantitative differences between the acute and chronic animals reached statistical significance. The data sets acquired at individual wavelengths were consistent with the increased collagen content reduced intra-tissue blood observed by histology in chronic animals. The large error bars could be due to intrinsic individual differences or imperfect light fluence compensation. Derived from the measurements at the three wavelengths, the ratios between collagen and hemoglobin contents, which are clinically expected to predict future outcomes, show significant differences between the two conditions.

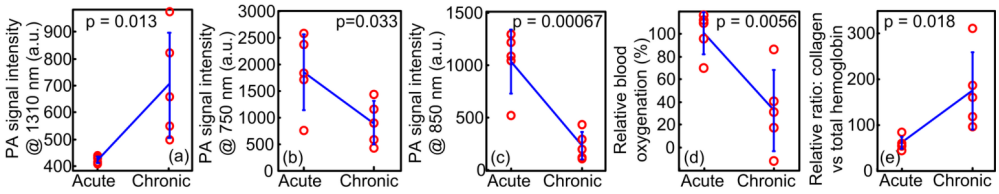

Fig. 7. Statistical results of the averaged factors derived from all the animals.

4. Discussion and future work

PA images at the individual optical wavelengths targeting specific molecular components are concordant with the corresponding gross images and histology of the affected intestine. The spectroscopic analysis of the PA images has demonstrated significant differences between the acute and chronic models of CD. The decreased oxygenation in the chronic animals is expected as intestinal fibrosis is often accompanied by local hypoxia [36, 37]. The observation of approximately 2-fold increase of PA signal intensity at 1310 nm in the chronic animals agrees with the results of our previous study [20]. Along with the decreased hemoglobin content, chronic animals have higher collagen/hb ratios. All the findings in PA imaging were consistent with histology.

The compensation for the wavelength-dependent optical attenuation is critical for the reliable spectroscopic analysis of the PA images. In this study, the thickness of the skin and muscle layers was measured by US. The optical attenuation was calculated using the optical properties reported in previous studies [31–33]. In addition, the limited bandwidth of the US data acquisition system dictates that the measurements at individual wavelengths are semi-quantitative. Under the assumption that each molecular component produces comparable frequency distributions in the PA signals, the calculation of the oxygenation and the collagen/hemoglobin ratio should have canceled the bandwidth effects and, therefore could produce more reliable measurements of diseased bowel.

The anesthesia of the animals assured that the same imaging plane was observed for spectral unmixing. The spatial averaging within the ROI followed by the temporal averaging of neighboring frames further minimized the uncertainty introduced by the respiratory motion. For a human subject study in the future, lasers with high repetition rate and quicker wavelength switching will be critical in order to avoid mismatch between the images at different wavelengths due to patient motion.

The translation of the imaging approach to human subjects also depends on the penetration of light at 1310 nm, where molecular components such as lipid, water as well as collagen in the skin and muscle, could substantially attenuate the optical energy in deep tissue. A recent study [38] and the optical properties shown in Table 1 show that the low scattering properties of the wavelengths longer than 1000 nm [32], combined with their high absorption, could lead to effective attenuation comparable to the 700-900 wavelength range.

Biomedical Optics EXPRESS

Figure 6 also demonstrated sufficient penetration through the rat bodies. In addition to attenuation compensation along the depth, normalization to the PA signals of neighboring features in the human body, such as the gall bladder or a major mesenteric artery, could be another promising solution. Studies on these issues will be included in our future works.

5. Conclusions

This study investigated the differentiation of inflammatory and fibrotic intestinal strictures using spectroscopic PA imaging in a rat model *in vivo*. PA measurements at individual wavelengths and the derived functional information have shown significant difference between the inflammatory and fibrotic animals, consistent with gross pathology and histology. By discriminating between inflammatory and fibrotic disease, PA imaging has clinical potential to longitudinally measure and monitor fibrosis, enable early diagnosis of both early and medically refractory disease, inform therapeutic modalities, and assess clinical response to drug therapy.

Funding

National Institute of Allergy and Infectious Diseases (1R21AI12209801A1); American Gastroenterological Association Boston Scientific Career Development Technology and Innovation Award, and Nation Cancer Institute (R43CA206756); National Natural Science Foundation of China (11574231, 61201425).

Disclosures

The authors declare that there are no conflicts of interest related to this article.